Biol. Cybern. 72, 519–526 (1995)

Biological Cybernetics

Characteristic nonlinearities of the 3/s ictal electroencephalogram identified by nonlinear autoregressive analysis

Nicholas D. Schiff, Jonathan D. Victor, Annemarie Canel, Douglas R. Labar

Department of Neurology and Neuroscience, The New York Hospital-Cornell Medical Center, 525 East 68 Street, New York City, NY 10021, USA

Received: 6 April 1994/Accepted in revised form: 18 November 1994

Abstract. We describe a method for the characterization of electroencephalographic (EEG) signals based on a model which features nonlinear feedback. The characteristic EEG 'fingerprints' obtained through this approach display the time-course of nonlinear interactions, rather than aspects susceptible to standard spectral analysis. Fingerprints of seizure discharges in six patients (five with typical absence seizures, one with complex partial seizures) revealed significant nonlinear interactions. The timing and pattern of these interactions correlated closely with the seizure type. Nonlinear autoregressive (NLAR) analysis is compared with other nonlinear dynamical measures that have been applied to the EEG.

1 Introduction

It is well recognized that epilepsy is a disturbance of neural circuits as well as an intrinsic disturbance of cells (Ebersole 1987). Although considerable attention has been paid to the cellular alterations in epilepsy (Prince 1978; Ebersole 1987), the circuit disturbances are not as well characterized. To characterize the circuit disturbances, a physiologically meaningful and numerically robust characterization of the time course of ictal electroencephalogram (EEG) patterns is required. These considerations motivated the development of a new analytical tool, nonlinear autoregressive analysis (NLAR) (Victor and Canel 1992). The purpose of this paper is to describe the application of NLAR to ictal EEG records, and to discuss the implications of these findings.

2 The nonlinear autoregressive model

Linear autoregressive (LAR) models (Gersh and Yonemoto 1977; Lopes da Silva 1982) characterize the EEG as a linear filter's response to a gaussian white noise input. Normal EEG activity is approximately gaussian (Elul 1969) and is well-characterized by LAR models (Siegel 1981; Wright et al. 1990). However, it fails to model key features of the ictal EEG, such as spiking behavior. This is because unidirectional spikes are inconsistent with the symmetry of a gaussian process.

Essentially, the NLAR model is a LAR model augmented by one or more quadratic interaction terms. Each such term represents the interaction of EEG values at two previous times. These nonlinear terms permit the description of nonlinear phenomena and deviations from gaussian processes. As with LAR and other models, description of the activity of populations of cortical neurons as recorded in the EEG does not specify the microdynamics of the underlying cellular elements (Wilson and Cowan 1972). Rather, the aim is to provide a window on the overall circuit properties and feedback interactions underlying ictal activity.

In this study, single-channel EEG recordings were examined from five patients with typical absence seizures and one patient with complex partial seizures. EEG segments exhibiting ictal activity were fitted by both LAR and NLAR models. In all cases, the NLAR model provided a more efficient fit than LAR models. Finally, the NLAR method is compared with other nonlinear dynamical measures applied to the EEG.

2.1 Patient characteristics and electrophysiologic recording

We analyzed EEG data from six patients (five with typical absence seizures, one with complex partial seizures during recovery from herpes simplex encephalitis) whose clinical characteristics are listed in Table 1.

Sixteen bipolar derivations of EEG were recorded via Ag/AgCl electrodes placed on the scalp according to the 10–20 system. These signals were recorded on a Telefactor (West Conshohocken, Penn.) telemetry apparatus (sampling at 250 Hz, high-pass filter at 0.3 Hz and low-pass filter at 70 Hz) along with a video image of the patient. Records which contained a clear artifact-free recording of ictal events were chosen for further analysis. The single channel chosen for analysis represented the clearest spike-wave complex by visual inspection. In patients 1–5, the 3/s spike wave discharge was generalized;

Correspondence to: N. D. Schiff

Table 1. Clinical characteristics of the patients studied

Patient no.	Ictal EEG pattern analyzed	Clinical seizure type	Medications	Age (years)
1	3/s spike wave	Typical absence	Valproate	12
2	3/s spike wave	Typical absence	None	10
3	3/s spike wave	Typical absence	Carbamazepine	6
4	3/s spike wave	Typical absence, complex partial	Carbamazepine	10
5	3/s spike wave	Typical absence, generalized convulsive	Valproate	10
6	Focal temporal repetitive sharp and slow waves	Complex partial	Phenytoin, phenobarbitol	50

Fp1–F7 was chosen for analysis unless otherwise noted. In patient 6, anterior temporal derivations were studied. This channel represented the clearest ictal morphology. The length of the segment from each ictal event varied from 4 to 8 s. In patients 1–3, 5, and 6, ictal events occurred during wakefulness. The electrographic ictal events analyzed from patient 4 occurred during sleep.

2.2 Strategy for autoregressive modelling

In a LAR model, a sample y_n of the EEG signal is represented as a sum of a random term, x_n, and a linear combination of values of the EEG at r prior times, $y_{n-1}, \ldots, y_{n-r}$:

$$y_n = x_n - \sum_{j=1}^{r} a_j y_{n-j} \tag{1}$$

The random terms x_n are assumed to be independently distributed.

In a NLAR model, we add quadratic terms to the above equation. A quadratic term allows EEG values at two prior times to interact. A model with all such possible terms takes the form

$$y_n = x_n - a_0 - \sum_{i=1}^{r} a_i y_{n-i} - \sum_{j=1}^{r} \sum_{k=1}^{r} c_{j,k} y_{n-j} y_{n-k} \tag{2}$$

In the model (2), an offset term a_0 is included. This term is required because the quadratic terms $c_{j,k}$ may shift the mean of the linear prediction.

We estimate the coefficients a_i and $c_{j,k}$ from the measured time series y_n by minimizing the unexplained (residual) variance V:

$$V = \langle x_n^2 \rangle \tag{3}$$

where $\langle\ \rangle$ represents an average over the data set. This minimization amounts to solving a system of linear equations strictly analogous to the Yule-Walker equations (Yule 1927; Gersh and Yonemoto 1977) of LAR models. (For further details, see Victor and Canel 1992.) We incorporate constant, linear, and quadratic terms in a common notation, and rewrite (2) as:

$$y_n = \sum_{k=1}^{J} c_k f_k(y_{n-1} y_{n-2}, \ldots, y_{n-r}) + x_n \tag{4}$$

We denote the current and previous values of the time series at step n by $Y_n = (y_n, y_{n-1}, \ldots,)$ and use the notation $f_j(Y_n) = f_j(y_{n-1}, y_{n-2}, \ldots, y_{n-r})$. Quantities such as $f_1, \ldots, f_J$ and $c_1, \ldots, c_J$ will be grouped as column-vectors $\vec{\mathbf{f}}$ and $\vec{\mathbf{c}}$. Here $\vec{\mathbf{f}}$ encompasses the LAR inputs y_{n-i} and the quadratic AR inputs $y_{n-j} y_{n-k}$ (as well as the constant term). Similarly, $\vec{\mathbf{c}}$ encompasses the LAR coefficients a_{n-i} and the quadratic AR coefficients $c_{n-j} y_{n-k}$ (as well as the constant coefficient a_0).

With these conventions, the model (2) may be rewritten

$$y_n = \vec{\mathbf{f}}(Y_n)^T \vec{\mathbf{c}} + x_n \tag{5}$$

and the residual variance (3) may be rewritten

$$V = \langle [y_n - \vec{\mathbf{f}}(Y_n)^T \vec{\mathbf{c}}]^2 \rangle \tag{6}$$

The Yule-Walker equations for the coefficients $\vec{\mathbf{c}}$ can be obtained by setting $\partial V / \partial c_j = 0$ for each c_j:

$$\langle \vec{\mathbf{f}}(Y_n) y_n \rangle = \langle \vec{\mathbf{f}}(Y_n) \vec{\mathbf{f}}(Y_n)^T \rangle \vec{\mathbf{c}} \tag{7}$$

Provided the matrix $\langle \vec{\mathbf{f}}(Y_n) \vec{\mathbf{f}}(Y_n)^T \rangle$ is nonsingular, values for $\vec{\mathbf{c}}$ may be calculated from:

$$\vec{\mathbf{c}} = \langle \vec{\mathbf{f}}(Y_n) \vec{\mathbf{f}}(Y_n)^T \rangle^{-1} \langle \vec{\mathbf{f}}(Y_n) y_n \rangle \tag{8}$$

Although in principle the above algorithm may be applied exactly as it stands, it suffers from two related weaknesses: there is an explosion of quadratic model parameters $c_{j,k}$, and the matrix in (8) may consequently be nearly singular. For a full quadratic model with 20 lags, there would be a total of 231 free parameters (1 offset, 20 linear, 210 quadratic). Though the issue of near-singularity can be addressed by an orthogonalization scheme (Korenberg 1988), in this work we take an approach which deals directly with the parameter explosion. We restrict consideration to models in which only a few of the terms $c_{j,k}$ are present. When only a single term is present, the NLAR model takes the form:

$$y_n = x_n - a_0 - \sum_{i=1}^{r} a_i y_{n-i} - c_{j,k} y_{n-j} y_{n-k} \tag{9}$$

This approach allows examination of the nonlinear dynamics without the need to fit a model with an excessive number of free parameters. Our strategy results in a model with 22 free parameters (1 offset, 20 linear, 1 quadratic). The residual variance for a single-term NLAR model necessarily depends on the choice of lags (j, k) for the single included nonlinear term. This dependence is a consequence of the nonlinear dynamics of the process which generates the original time series, and we call this dependence the 'NLAR fingerprint.'

2.3 Determination of significance of AR terms

In any AR model, adding a new term never increases the residual variance. Thus, reduction of residual variance per se does not imply a significantly improved model. For LAR models, Akaike (1974) proposed a statistical criterion to determine when the amount of reduction in

residual variance is sufficient to justify the inclusion of an additional term. The Akaike criterion (AIC) is the sum of two quantities:

$$\mathrm{AIC} = N \log V + 2J \tag{10}$$

where N represents the number of data points, J is the number of model terms, and V is the residual variance. The AIC balances the cost of the number of parameters ($2J$) against the amount of information in the model (reduction in V). Akaike's derivation of the AIC (Akaike 1974) rested on the fact that the LAR parameters estimated from the Yule-Walker equations are the maximum-likelihood estimates. But in NLAR models, parameter estimates from the Yule-Walker equations are not maximum likelihood estimates, since the x_n's are not assumed to be distributed in a gaussian fashion. Nevertheless, the reduction in variance ΔV resulting from the addition of a single nonlinear term with coefficient c_j can be used as a measure of the significance of that term. This is because at a given level of significance p, the confidence limit for c_j for the nonlinear term does not include 0 when

$$N\Delta V/V > K \tag{11}$$

where K is the square of the critical value of the t-statistic (Victor and Canel 1992). The criterion (11) for $K = 2$ corresponds to the AIC (10).

3 Results

3.1 Robustness of NLAR model

The analysis procedure for an EEG segment consisted of the following steps. In the first step, we fitted LAR models to a data segment via (8). In the second step, we fitted multiple nonlinear models (9), one for each possible pair of lags (j, k), as described above. The lags j and k were allowed to range from 1 to 20 sampling intervals (see below). We then construct the nonlinear fingerprint, a contour map, which displays the residual variance V for each pair of lags (j, k).

3.2 NLAR modelling of one seizure record

In this section, we go through the analysis of one data segment in detail. Channel 7 (Fp1–F7) was chosen for analysis because the spike wave discharge was prominent and the segment was free of artifact.

We next used (1) to generate LAR models with a successively increasing number J of linear terms. Data digitized at the initial sampling rate of 250 Hz was resampled at 125 Hz (2:1) prior to LAR analysis, so that each lag represented 8 ms. Figure 1, shows the residual variance (V), relative AIC values, and the fractional reduction in variance ($N\Delta V/V$) for LAR models with 1–20 linear terms. For these models, the AIC showed a minimum at $J = 6$ lags. This model accounted for 82.40% of the variance. After a slight rise in the AIC value, addition of further lags resulted in small decreases in the criterion for 13–20 lags. With $J = 20$ lags, the LAR model accounted for 83.26% of the variance, which represents a very slight improvement over the 6-lag LAR model.

In the second step of the analysis, a single quadratic (or bilinear) interaction term was added into the otherwise linear AR model. The Yule-Walker equations for 22 terms (an offset, 20 linear terms, and a single quadratic or bilinear interaction term) were used to calculate the coefficient $c_{j,k}$ and the resulting reduction in the variance $\Delta V_{j,k}$. This calculation was performed separately for all values of j and k in the range from 1 to 20, to explore the space of nonlinear signal interactions. The number of lags in the LAR model was held fixed at 20 to allow all quadratic terms to be compared on an equal footing. (If a nonlinear term were introduced at a lag for which no linear term were present, then the absence of a linear term per se might bias the estimate of the contribution of the nonlinear term; Victor and Canel 1992.) Contour maps were generated for the reduction in residual variance $\Delta V_{j,k}$ (Fig. 2). In the contour map (Fig. 2) of the reduction in residual variance $\Delta V_{j,k}$, we have indicated statistical significance of the quadratic terms by placing a small solid dot at the coordinates (j, k) for which the reduction in variance satisfies (11) with $K = 4$. This is a stricter criterion than the AIC, which corresponds to $K = 2$.

One prominent feature of the NLAR fingerprint (Fig. 2) for this segment is a ridge parallel to the main diagonal running from (4, 7) to (8, 11). Since at the sampling rate of 125 Hz each lag represents 8 ms, this pattern indicates an interaction of signals separated by roughly 24 ms from times 32 ms to 64 ms in the past. The other local minima of variance were at (3, 2), (8, 17), (15, 15) and (1, 8).

The range of reduction in variance achieved with the addition of specific nonlinear interaction terms is shown over the symbol Q in Fig. 1A. The reduction of the AIC accompanying inclusion of a single quadratic term varied from none [lags (2, 16)] to substantial [115 for lags (3, 2)]. The $N\Delta V/V$ term correspondingly ranged from 2 [lags (2, 16)] to 132 [lags (3, 2)]. The NLAR model with the single term at lags (3, 2) accounted for 86.79% of the total variance. That is, this one-term NLAR model accounted for 21% of the variance which remained after the 20-term LAR model was fitted.

To determine whether the pattern and location of features in the NLAR fingerprint were tied to the sampling rate or rather to the time interval represented by the lags, we performed the analysis described above on the same data segment sampled at intervals of 12 and 16 ms. The features in the 12 and 16 ms fingerprints (not shown) matched the features in the 8-ms fingerprint provided that the amount of time represented by each lag is taken into account. For example, there was a minimum at lags (9, 1) in the 8-ms fingerprint, which corresponds to (72 ms, 8 ms). This feature matched a minimum in the 12-ms fingerprint between lags (6, 1) and lags (7, 1), which corresponds to (78 ms, 12 ms). It also matched a minimum in the 16-ms fingerprint at lags (5, 1), which corresponds to (80 ms, 16 ms). The only major minimum in the 8-ms fingerprint which was not preserved in the fingerprints sampled at coarser intervals is the minimum at

lags (3, 2). Presumably, the failure of the coarser data sampling to resolve this interaction is a consequence of its brief time course. Other than this exception, this analysis shows that the features in the nonlinear fingerprints represent interactions that are inherent in the time structure of the data and are not a consequence of the sampling rate.

We carried out the analysis described above for a second seizure event recorded in patient 1. The dependence

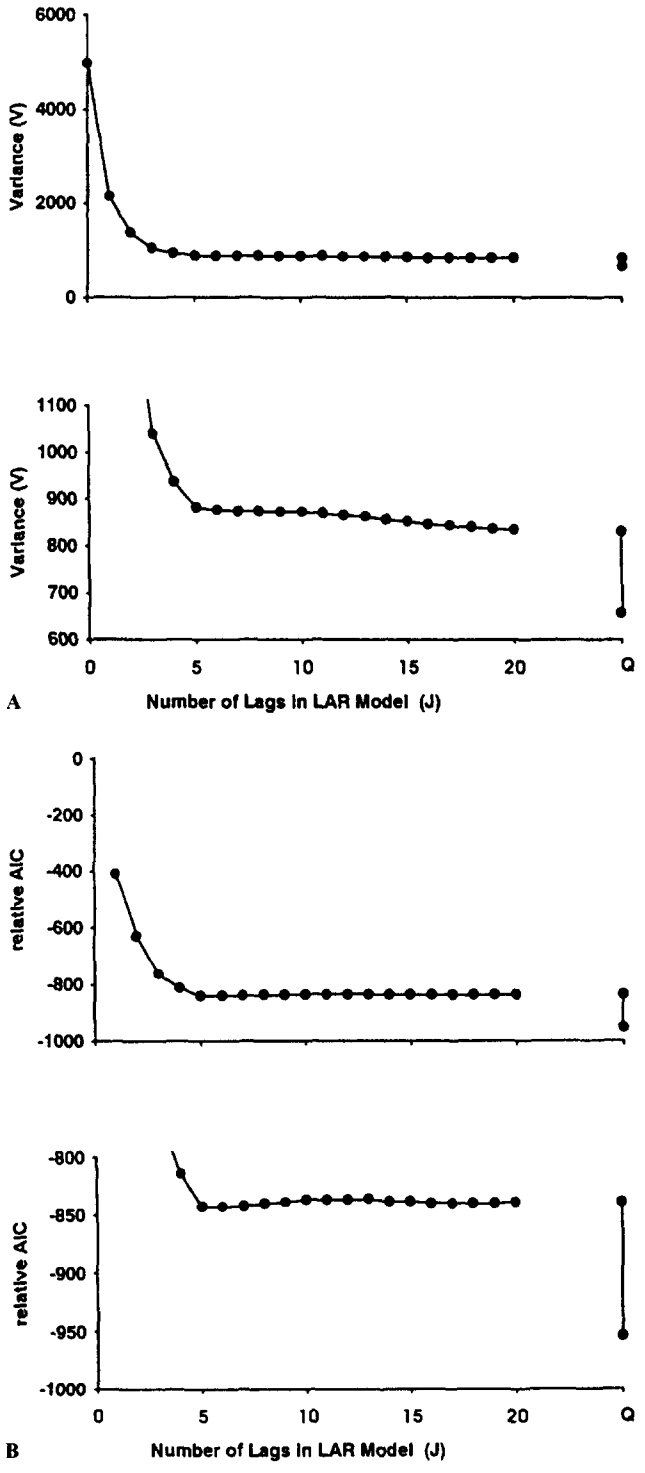

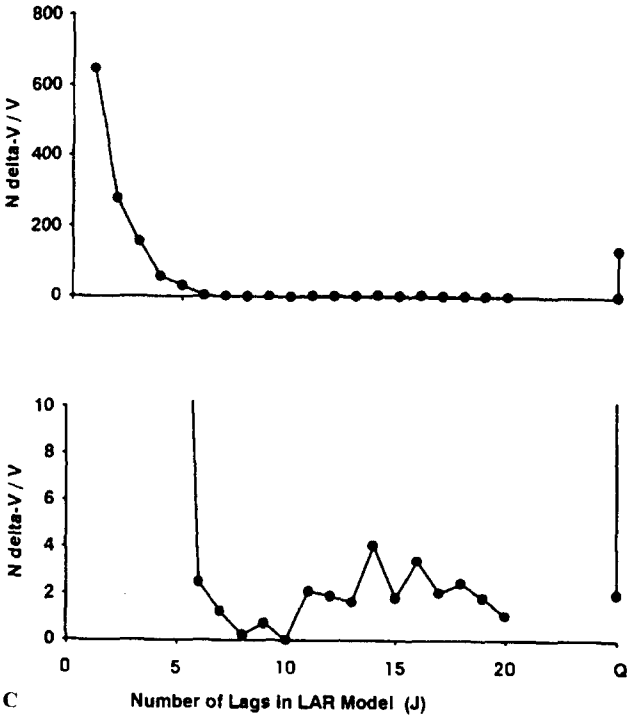

Fig. 1. **A** Residual variance (μV^2) for linear (*left section* of *abscissa*) and nonlinear (Q) autoregressive (NLAR) models. The two points above the abscissa Q indicate the range of residual variances encountered among all NLAR models. **B** Reduction in the Akaike criterion (AIC) for linear and NLAR models. **C** $N\Delta V/V$ for linear and NLAR models. Terms corresponding to $N\Delta V/V > 4$ are statistically significant at $P < 0.05$ by the method of Victor and Canel (1992). Data from channel 7 (Fp1–F7).

of the residual variance (V), AIC, and the fractional reduction in variance ($N\Delta V/V$) on the number of lags in LAR models was very similar to that seen in the first data set. Although the relative amounts of variance reductions differed somewhat, the overall pattern and position of the fingerprint features were remarkably similar in the two discharges.

3.3 Comparison across patients

The analysis described above was applied to ictal records from the other four patients with 3/s seizures (Table 1). Only fragmented 3/s discharges were recorded in patient 2. Nevertheless, the NLAR fingerprint obtained from these fragments (Fig. 3A) was markedly similar to that of patient 1: minima at lags (8, 1), (8, 17), and along a ridge parallel to the diagonal from lags (3, 6) to (6, 9). The NLAR fingerprint obtained from 3/s discharges of patient 3 (Fig. 3B) was somewhat different from that of patients 1 and 2, but nevertheless showed minima at lags (9, 1) and (8, 17). The parallel ridges off the diagonal were shifted up to lags (8, 10).

The NLAR fingerprints obtained from patients 4 and 5 are different from those of patients 1–3. The fingerprint for patient 4 (Fig. 4A) displayed only two of the prominent minima seen in patients 1–3 [lags (8, 1) and lags (8, 17)] and did not have the ridges. The fingerprint from patient 5 (not shown) had a steep minimum at (8, 17),

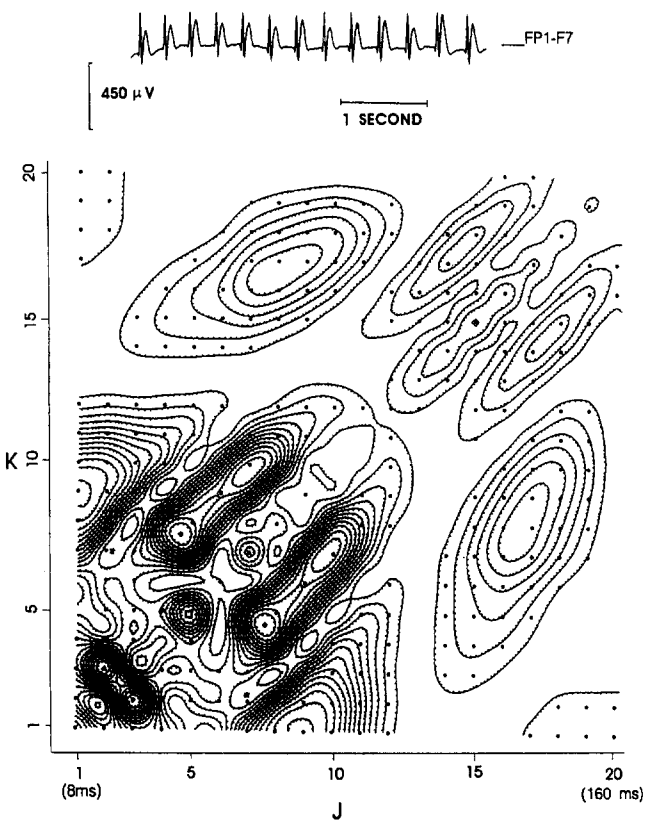

Fig. 2. Nonlinear autoregressive (NLAR) fingerprint derived from an ictal discharge recorded from patient 1. This is a contour map of the reduction in residual variance $\Delta V_{j,k}$ for NLAR models containing a single nonlinear term at lags (j, k). Each time unit (j or k) represents 8 ms. *Tickmarks* point downhill, and each *contour line* represents 0.25% of the variance. Statistical significance is indicated by placing a *small, solid dot* at the coordinates (j, k) for which the reduction in variance satisfies $N\Delta V_{j,k}/V > 4$. The discharge analyzed is displayed above the contour map. Data from channel 7 (Fp1–F7).

which corresponds to a feature seen in patients 1–4. Another minimum in this fingerprint, at lags (16, 16), may correspond to the minimum seen in the fingerprints from patient 1 at lags (15, 15). The fingerprint of patient 5 also lacked the off-diagonal ridges seen in patients 1–3. Of note, patients 4 and 5 show an atypical morphology of the 3/s discharge (more sharp waves than spike waves), and patient 5 has a congenital brain malformation (Dubowitz syndrome). Patients 1–3 have typical 3/s spike waves seen in petit mal epilepsy.

An NLAR fingerprint derived from a complex partial seizure in patient 6, as recorded at T1–T2, is shown in Fig. 4B. This seizure discharge is approximately periodic at 2.5 Hz. The NLAR fingerprint has little in common with the other fingerprints. There were no minima corresponding to interactions at lags greater than 80 ms (lag 10), and there were no ridges parallel to the diagonal. The deepest minimum was at lags (5, 6), corresponding to (40 ms, 48 ms).

Table 2 summarizes the major features of fingerprints obtained from 3/s seizure records. Fingerprints from all patients (1–5) had a prominent minimum at lags (8, 17), which corresponds to (64 ms, 136 ms). Fingerprints from

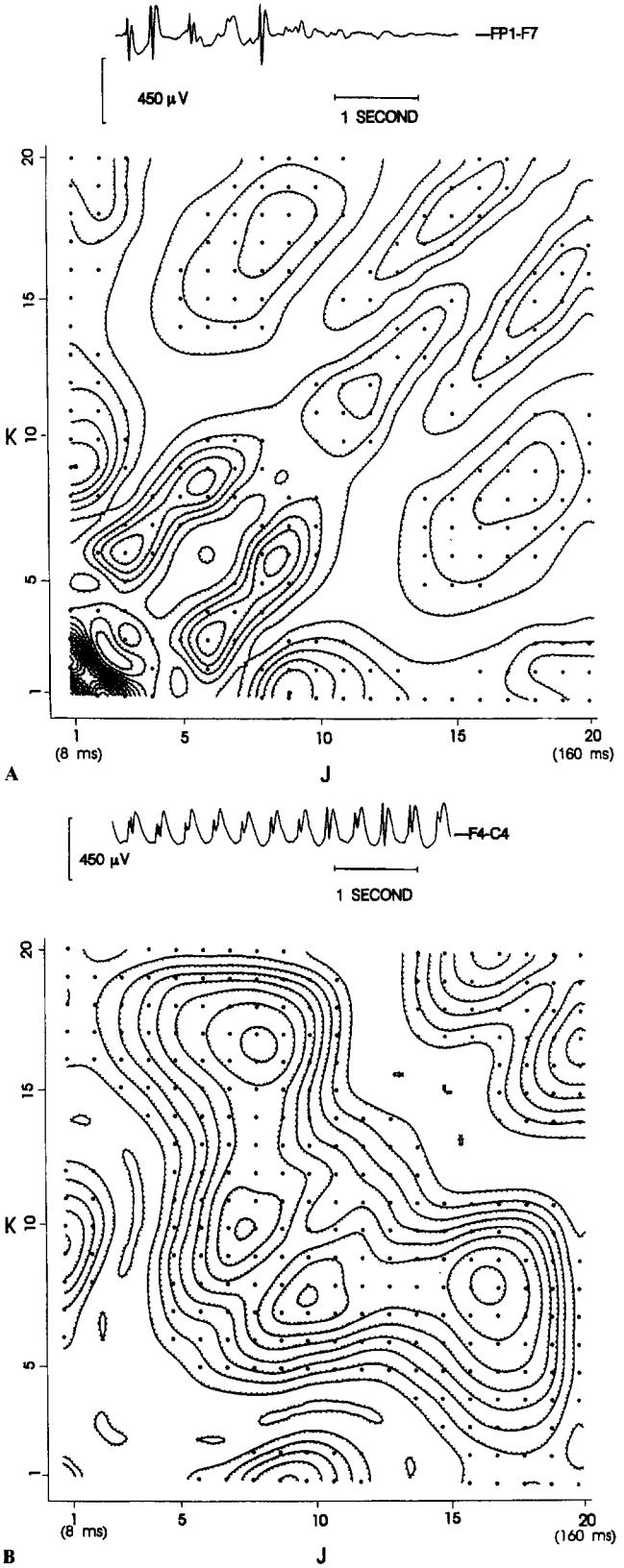

Fig. 3. **A** NLAR fingerprint derived from a fragmented ictal discharge recorded from patient 2. Each *contour line* represents 0.1% of the variance. For other plotting conventions as in Fig. 2. The discharge analyzed is displayed above the contour map. **B** NLAR fingerprint derived from an ictal discharge recorded from patient 3. Each *contour line* represents 0.05% of the variance. Other plotting conventions as in Fig. 2. The discharge analyzed is displayed above the contour map.

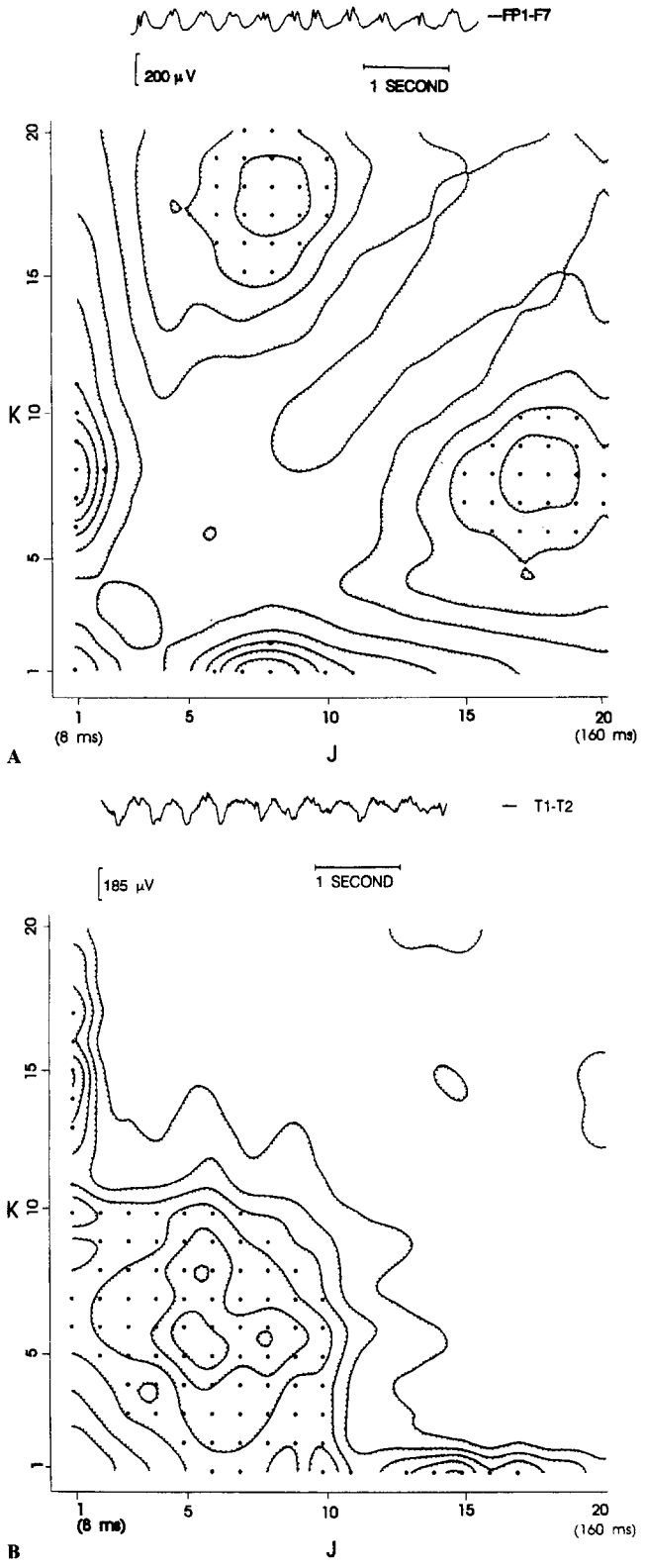

Fig. 4. **A** NLAR fingerprint derived from an ictal discharge recorded from patient 4. Each *contour line* represents 0.01% of the variance. Other plotting conventions as in Fig. 2. The discharge analyzed is displayed above the contour map. **B** NLAR fingerprint derived from an ictal discharge recorded from patient 6. Each *contour line* represents 0.025% of the variance. Other plotting conventions as in Fig. 2. The discharge analyzed is displayed above the contour map. Note that both seizures have similar periodicity but clearly different dynamics reflected in the NLAR fingerprint.

four of the five patients (1–4) had a prominent minimum at lags (1, 8) or (1, 9). Three of the five patients (patients 1–3) showed the striking feature of deep ridges parallel to the diagonal. The similar location of the minima stands in contrast to the large differences in the percentage of the variance explained by LAR and NLAR models. None of these minima corresponded to features in the NLAR fingerprint derived from a complex partial seizure in patient 6.

4 Discussion

4.1 Summary of results

We have shown how NLAR models may be applied to the ictal EEG to create a fingerprint of the nonlinear dynamics, without incurring an explosion of parameters or other pitfalls associated with previous methods of nonlinear analysis of the EEG. Similarities and differences in the fingerprint pattern obtained across patients correlated with their epilepsy diagnosis. For patients with only typical absence seizures (patients 1–3), the main features of the nonlinear fingerprint were minima centered at lags (64 ms, 136 ms), (8 ms, 72 ms), and a ridge of lags separated by 24 ms, ranging from 40 ms to 60 ms in the past. For patients with typical absence seizures as part of a more extensive seizure disorder (patients 4 and 5), the fingerprints had some but not all of these features. The nonlinear fingerprint of a complex partial seizure had no resemblance to this pattern and lacked the minimum at lags (64 ms, 136 ms) which were present in all patients with 3/s seizures. The similarities and differences in the nonlinear fingerprints in these patients thus correlated with the similarities and differences in their epilepsy diagnoses.

4.2 Comparison with other approaches to nonlinear dynamics

Several parametric and nonparametric methods of characterization of nonlinear dynamics have been applied to the EEG. All of these approaches share one feature with the present approach: they characterize aspects of the discharge that are independent of the power spectrum, or cross-correlation. However, there are many significant differences.

Babloyantz and Destexhe (1986), Mayer-Kress (1987), and others have used dimension formalism to examine the EEG and the 3/s discharge. A related approach to the identification of nonlinear dynamics is based on the use of surrogate data sets (Casdagli et al. 1991; Theiler et al. 1991). In contrast to the present approach, these approaches focus on global dynamical behavior. However, rigorous measurement of dimension requires high signal-to-noise, extensive data sets, and stationarity. Furthermore, it is difficult to use a single number, such as an experimentally determined dimension, to test dynamical models; the nonlinear fingerprints presented here do lend themselves to such interpretations (Schiff et al. 1994).

Table 2. Summary of autoregressive models of ictal discharges. Two data segments per patient were analyzed. Location of minimal-variance NLAR models is specified in terms of lag coordinates (j, k), where each lag unit corresponds to 8 ms.

Patient no.	Segment no.	Location of prominent minima					Total V	%RV(L)	%RV(N)
1	1	(3, 2)	(5, 8)	(9, 1)	(8, 18)	(15, 15)	4976	16.7	13.5
	2	(3, 2)	(5, 8)	(9, 1)	(8, 17)	(15, 15)	5474	17.3	14.2
2	1		(6, 8)	(9, 1)	(8, 17)	(12, 12)	2964	11.8	10.6
	2		(7, 10)	(9, 1)	(9, 18)		4313	11.8	9.6
3	1		(6, 8)	(9, 1)	(6, 15)		7009	4.9	4.5
	2			(9, 1)	(8, 17)		6137	3.0	2.8
4	1			(9, 1)	(8, 17)		1393	2.50	2.45
	2			(9, 1)	(8, 17)		1380	2.00	1.95
5	1				(8, 20)	(16, 16)	1795	7.0	6.5
	2				(8, 18)	(16, 16)	1832	3.4	3.0
6	1						1592	8.2	8.0

Total V, total variance (μV^2); %RV (L), percentage of variance remaining after 20-term LAR model; %RV (N), percentage of variance remaining after augmentation of LAR model by the optimum single quadratic term

The information one can obtain from the NLAR fingerprint is in principle independent of the information one can obtain from the dimension. Dimension is a topologically invariant feature of the dynamics (Farmer et al. 1983; Feigenbaum 1983); it therefore is not altered by transformations (such as non-linear filters) which change parametric measures such as the NLAR fingerprint. On the other hand, dimension reflects global properties; the NLAR fingerprint (at least in the present application) reflects local properties.

The original motivation for the NLAR fingerprint was to characterize in a systematic fashion deviations from the null hypothesis that the signal is a linear transformation of gaussian white noise. That is, the NLAR fingerprint is based on third-order moments, calculated in the time domain, which are expected to be zero if the signal satisfies this null hypothesis. The bispectrum is a related approach, based on third-order moments calculated in the frequency domain. Under the null hypothesis, the bispectrum is zero. From the relatively limited use of the bispectrum in EEG analysis, it appears that this procedure is not an efficient one: many records must be averaged, and data must be smoothed, to obtain a meaningful bispectrum (Lopes da Silva 1982). The apparent inefficiency of the bispectrum in comparison to the nonlinear fingerprint described here is likely related to the greater efficiency of AR models in comparison with Fourier methods in the calculation of the power spectrum (Akaike 1974; Gersh and Yonemoto 1977; Lopes da Silva 1982).

Finally, Korenberg (1988) has proposed a procedure to obtain the coefficients of an NLAR model with all terms included. Korenberg's method of orthogonalization avoids the numerical pitfalls of inverting a large, nearly singular matrix. However, it does not avoid the problem of the explosion of the number of nonlinear parameters.

Acknowledgements N.S. was supported by a Howard Hughes Medical Student Research Training Fellowship and a medical student fellowship from the Epilepsy Foundation of America. J.V. was supported in part by EY7977 and EY9314 from the National Eye Institute and the Klingenstein Foundation. We thank Mary Conte for expert technical assistance.

References

Akaike H (1974) A new look at statistical model identification. IEEE Trans Auto Control AC-19:716–723

Babloyantz A, Destexhe A (1986) Low-dimensional chaos in an instance of epilepsy. Proc Natl Acad Sci USA 83:1313–1317

Casdagli M, Des Jardins D, Eubank S, Farmer JD, Gibson J, Hunter N, Theiler J (1991) Nonlinear modeling of chaotic time series: theory and applications. (Los Alamos preprint: LA-UR-91-1637) Los Alamos National Laboratory, Los Alamos

Ebersole JS (1987) Physiological substrates of normal and abnormal EEG activity. In: State of the science in clinical EEG and electroencephalography. American Electroencephalographic Society

Elul R (1969) Gaussian behavior of the electroencephalogram: changes during the performance of a mental task. Science 164:328–331

Farmer JD, Ott E, Yorke JA (1983) The dimension of chaotic attractors. Physica 7D:153–180

Feigenbaum M (1983) Universal behavior in nonlinear systems. Physica 7D:16–39

Gersh W, Yonemoto J (1977) Parametric time series models for multivariate EEG analysis. Comp Biomed Res 10:113–125

Korenberg MJ (1987) Functional expansions, parallel cascades, and nonlinear difference equations. In: Marmarelis VZ (ed) Advanced methods of physiological system modelling. University of Southern California, Los Angeles

Korenberg MJ (1988) Identifying nonlinear difference equations and functional expansion representations: the fast orthogonal algorithm. Ann Biomed Eng 16:123–142

Lopes da Silva FH (1982) Computer-assisted EEG diagnosis: pattern recognition in EEG analysis, feature extraction and classification. In: Niedermeyer E, Lopes da Silva FH (eds) Electroencephalography. Urban and Schwarzenberg, Baltimore, pp 713–732

Mayer-Kress G (1987) Application of dimension algorithms to experimental chaos. (Los Alamos preprint LA-UR-87-1030) Los Alamos National Laboratory, Los Alamos

Neidermeyer E (1983) Epileptic seizure disorders. In: Niedermeyer E, Lopes da Silva FH (eds) Electroencephalography Urban and Schwarzenberg, Baltimore, pp 339–428

Prince DA (1978) Neurophysiology of epilepsy. Annu Rev Neurosci 1:395–415

Siegel A (1981) Stochastic aspects of the generation of the electroencephalogram. J Theor Biol 92:317–339

Theiler J, Galdrikian B, Longtin A, Farmer JD (1991) Testing for nonlinearity in time series: the method of surrogate data. (Los Alamos National Laboratory Preprint LA-UR-91-3343) Los Alamos National Laboratory, Los Alamos

Victor JD, Canel A (1992) A relation between the Akaike criterion and reliability of parameter estimates, with application to nonlinear autoregressive modelling the ictal EEG. Ann Biomed 20:167–180

Wilson HR, Cowan JD (1972) A mathematical theory of the functional dynamics of cortical and thalamic nervous tissue. Kybernetik 13:55–80

Wright JJ, Kydd RR, Sergejew AA (1990) Autoregression models of the EEG. Biol Cybern 62:201–210

Yule GU (1927) On a method of investigating periodicities in disturbed series with special reference to Wolfer's sunspot numbers. Philos Trans R Soc Lond A 226:267–298